



Improvement of the coagulation–flocculation process using graphene oxide for ciprofloxacin removal from surface water

Mahshid Maddah Safae Torogh^a, Amir Azizi^b, Mehdi Amirsadeghi^c, Majid Baghdadi^{a,*}

^aSchool of Environment, College of Engineering, University of Tehran, Tehran, Iran, P.O. Box: 1417853111, Tel. +98 21 61113171; Fax: +98 21 66407719; emails: m.baghdadi@ut.ac.ir (M. Baghdadi), msafae91@alumni.ut.ac.ir (M.M. Safae Torogh)

^bDepartment of Chemistry, Faculty of Science, Arak University, Arak, Iran, email: a-azizi@araku.ac.ir

^cAnimal Science Research Institute of Iran, Agricultural Research, Education and Extension Organization (AREEO), Karaj, Iran, email: m.amirsadeghi@areeo.ac.ir

Received 9 February 2021; Accepted 12 September 2021

ABSTRACT

For the first time, the effect of the chemical reduction of graphene oxide (GO) on the adsorption of ciprofloxacin (CIP) was investigated. Furthermore, GO was applied in the coagulation–flocculation process for CIP adsorption from surface water. Moreover, the application of Fe_3O_4 for enhancing sedimentation rate and reducing sludge volume was investigated. The results showed that the functional groups of GO have a significant impact on the adsorption of CIP, and chemical reduction of GO resulted in reducing the adsorption capacity. The analysis of variance showed that the quadratic model was consistent with the experimental data. Furthermore, pH and GO dosage were more effective than $\text{FeCl}_3 \cdot 6\text{H}_2\text{O}$ in removal efficiency. Under the optimum conditions (GO dose: 0.08 mg L^{-1} , pH: 6.0, and $\text{FeCl}_3 \cdot 6\text{H}_2\text{O}$: 10 mg L^{-1}) removal efficiency of 83.1% was achieved for the sample containing 10 mg L^{-1} of CIP. The adsorption efficiency increased by increasing total dissolved solids to 800 mg L^{-1} . The maximum removal efficiency of 95.3% was achieved at the contact time of 15 min. The Langmuir isotherm model was able to predict the experimental adsorption data and indicated a maximum capacity of 185 mg g^{-1} . The sedimentation kinetic data were appropriately fitted to the pseudo-first-order model. Finally, the reusability of the adsorbent was studied, and the results showed a 65% reduction in removal efficiency after three cycles. In conclusion, the application of graphene oxide in the coagulation–flocculation process enhances the performance of the unit for adsorption of ciprofloxacin. Furthermore, the magnetite nanoparticles have a significant impact on the reduction of sludge volume and increase sedimentation rate.

Keywords: Graphene oxide; Ciprofloxacin; Coagulation–flocculation; removal; Surface water

1. Introduction

The presence of pharmaceuticals in wastewater is considered an emerging environmental problem because of their adverse effects on the aquatic ecosystem even at low concentrations [1,2]. Antibiotics can reach the environment in various ways, including animal or human wastes and effluents from pharmaceutical manufacturing plants [3].

Among the pharmaceuticals, antibiotics have received a great deal of attention because of their serious risks to the environment [4]. Fluoroquinolones (FQs) are synthetic antibiotics, which are one of the main drugs applied worldwide. FQs are not biodegradable. Hence, the presence of the FQs in aquatic environments has become a growing concern [5]. Ciprofloxacin (CIP), as the third generation of FQs, is not biodegradable [6]. Unfortunately, about 30%–90% of CIP is excreted in unmetabolized form or as active metabolites,

* Corresponding author.

thereby entering wastewater [7]. It also is present in pharmaceutical wastewaters [8]. It is reported that the concentration of CIP in wastewater could increase to 50 mg L⁻¹ [9–11]. CIP released in the environment may contaminate the drinking water and aquatic ecosystems even at low concentrations.

Advanced oxidation processes (AOPs), including ozonation, electro-activated persulfate oxidation, photocatalytic, and electro-Fenton processes, have been reported for the removal of pharmaceuticals from water and wastewater [12–15]. Degradation of metformin in pharmaceutical wastewater using the electro-Fenton process has been reported as a rapid and efficient removal approach [16]. However, the main disadvantage of AOPs is the formation of by-products [17]. As a consequence, the toxicity of treated wastewater can be increased. Benzoquinone has been reported as an intermediate of the degradation of aromatic compounds [18]. Therefore, the application of such a technique is limited.

Nowadays, adsorption is one of the main methods used for the removal of pharmaceuticals from wastewater. The benefits of such a technology are the high capability to remove many pollutants, high performance, low cost, easy operation, and simple recovery for reuse. Some factors, for example, the surface areas of the adsorbent and incorporated functional groups affect the adsorption efficiency [19]. Several studies have recently reported the removal of CIP from wastewater by using a variety of adsorbents. For example, Li et al. [20] investigated the adsorption of CIP with kaolinite. The maximum adsorption capacity of this adsorbent was estimated to be up to 19 mmol kg⁻¹. Jiang et al. [21] used birnessite and estimated a maximum adsorption capacity of 72 mg g⁻¹. Genç et al. [22] applied bentonite for CIP removal and observed a maximum adsorption capacity of 147.06 mg g⁻¹. Balarak et al. [23] studied the mechanism and kinetics of red mud in the removal of CIP, and the results showed the highest removal efficiency of 96.5%.

The coagulation–flocculation process is one of the traditional methods used in urban and industrial wastewaters treatment, and nowadays this process is implemented widely for reducing turbidity, eliminating organic matter, and inorganic pollutants [24]. Recent studies have pointed out the inefficiency of the conventional processes for removing micropollutants (MPs) [25–27]. Matamoros and Salvadó [28] studied the removal of several MPs in a coagulation/flocculation-lamella clarifier. The results showed that the hydrophobicity of the compounds ($\log K_{ow}$) is effective on the removal of MPs in a coagulation–flocculation process. The removal efficiencies in the range of 20%–50% were obtained for the MPs with $\log K_{ow} \geq 4$ at pH 7–8 [28]. Therefore, it can be concluded that CIP with a low K_{ow} (1.9) cannot be efficiently removed using the coagulation–flocculation process [29].

Lately, some adsorbents have been developed for CIP adsorption from water samples [4]. In this respect, the effectiveness of graphene oxide (GO) has been widely studied for the removal of wastewater pollutants [30–33]. Graphene oxide decorated with zeolitic imidazolate framework (ZIF-8) and pseudo-boehmite has been reported as an ultra-high adsorption capacity for diclofenac adsorption from hospital effluents [34]. It has been reported

that easy-to-prepare GO nanocomposites with enhanced adsorption performance for water treatment [35]. GO can be a proper adsorbent because of its functional groups (carboxyl and hydroxyl) and high surface area [36]. Nevertheless, GO has not been practically used for water treatment because of its high dispersibility in aqueous solutions and small particle size, which makes its separation difficult from treated wastewater. As a solution to this problem, magnetic graphene oxide (MGO) has been suggested, which can be easily separated by an external magnetic force after treatment. Different methods have been reported for preparing MGO [36,37]. However, these methods cannot be easily controlled and they are multistep. In addition, magnetic nanoparticles reduce the GO adsorption capacity due to a decline in the surface area and occupation of the active sites [38]. An efficient technology that can be used to eliminate these problems is “In Situ Sludge Magnetic Impregnation” (ISSMI) [39], which increases the sludge sedimentation rate and reduce the sludge volume index.

In this study, for the first time, the effect of the chemical reduction of GO on the adsorption of CIP was investigated. In addition, GO was applied to adsorb the CIP from the surface water by the ISSMI technique incorporated in the coagulation–flocculation process to separate the GO nanosheet after the adsorption process. Fe₃O₄ nanoparticles were used to prepare the magnetic sludge, thereby enhancing sludge separation and decreasing the sludge volume. The Box–Behnken design was applied to optimize the effective parameters, such as adsorbent dosage, initial pH, and coagulant amount to achieve the maximum CIP removal.

2. Experimental

2.1. Materials

Graphite fine powder applied in this work was purchased from Loba Chemie (India). Other chemicals including ammonia solution (25% wt), iron salts (FeCl₃·6H₂O and FeCl₂·4H₂O), potassium nitrate (99% wt), potassium permanganate (97% wt), hydrogen peroxide (30% wt), and sulfuric acid (98% wt) were procured from Merck (Darmstadt, Germany) and applied for the preparation of Fe₃O₄ nanoparticles and graphene oxide (GO). Hydrazine (99% wt) was used to reduce GO. Sodium hydroxide (97% wt) and hydrochloric acid (37% wt), also obtained from Merck, were applied to adjust the initial pH of solutions. Ciprofloxacin (C₁₇H₁₈FN₃O₃) was obtained from Ronak Pharmacology Co., Tehran, Iran. All the reagents and chemicals used in this study were of synthetic grade or higher. Deionized water was applied for all the experiments.

2.2. Surface water sample

In this research, a real surface water sample was used to conduct the experiments. The surface water was taken from the Karaj River (Karaj, Iran). Table 1 presents the analysis of the collected sample. The samples were spiked with CIP to evaluate the performance of the proposed method.

2.3. Preparation of GO, rGO, and Fe₃O₄ nanoparticles

Fine graphite powder (extra pure) was applied to synthesize GO by the Hummers approach [40]. The chemical

Table 1
Analysis of the surface water

Parameter	Quantity
pH	7.5
Electrical conductivity, mg L ⁻¹	282
Total suspended solids, mg L ⁻¹	204
Turbidity, NTU	209

Obtained from Karaj River (Karaj, Iran).

co-precipitation method was used for preparing the Fe₃O₄ nanoparticles [41]. For more detail see the supplemental material.

A stock solution of hydrazine (2,000 mg L⁻¹) was prepared and used for the reduction of GO. The desired values of hydrazine were poured into a 250 mL flask containing 100 mL of deionized water, and then 0.06 g of synthesized GO was poured into the solution. The solution was constantly mixed for 3 h at 80°C.

2.4. Analytical methods

An HPLC (Agilent, 1100) with a C18 column (5 mm, 4.6.250 mm) and equipped with a UV detector at 276 nm was used for the determination of CIP concentration. A mixture of water/acetonitrile (40:60 v/v) was applied as the mobile phase, which was delivered at 1.0 mL min⁻¹. The samples were filtered on a polytetrafluoroethylene (PTFE) filter (0.2 mm) and subsequently were injected by a 20 mL injector loop. Based on standard method 5220D [42], a spectrophotometric method using a UV/VIS spectrophotometer (HACH, DR 5000, USA) was used to determine the chemical oxygen demand. The total suspended solids (TDS) were measured in compliance with standard method 2540 D [42]. pH was measured with a pH meter (Metrohm 691, Switzerland) equipped with a combined glass saturated calomel electrode.

2.5. Characterization of GO and Fe₃O₄ nanoparticles

The crystal structure of the GO and Fe₃O₄ nanoparticles were analyzed using an X-ray powder diffraction instrument (XRD, Bruker, D8 ADVANCE) with Cu K α radiation X-ray source. A scanning electron microscopy (SEM, Zeiss, EM 900) was used for obtaining the SEM images. The magnetic properties of Fe₃O₄ were measured by a vibrating sample magnetometer (VSM) with a magnetic field of 10,000 Oe. Also, to obtain information about possible bonds of GO, reduced graphene oxide (rGO), and Fe₃O₄ nanoparticles, Fourier transform infrared (FTIR) spectrometer (Bruker, Tensor 27) was utilized, using KBr pellets within 400–4,000 cm⁻¹. Zeta potential data were obtained using a Malvern Zetameter (Malvern, ZEN3600). Surface charge of GO was measured by zeta potential meter (Zetasizer, Malvern, UK) at the pH of 8.

2.6. Experimental design and data analysis

In this research, the Box–Behnken design was utilized as the most popular response surface methodology (RSM)

Table 2
The independent variable parameters and their values

Variable	Factor	Levels and values		
		(-1)	(0)	(+1)
Solution pH	x_{pH}	3.0	6.5	10.0
[GO] dose, mg L ⁻¹	x_{GO}	4.0	42.0	80.0
[FeCl ₃ ·6H ₂ O] concentration, mg L ⁻¹	x_{FeCl_3}	1.0	5.5	10.0

to find the optimum conditions for the critical parameters. The number of required tests (N) was estimated by $N = 2k(2k - 1) + N_0$ where k is the number of variables and N_0 is the number of the central points. The variable parameters were adsorbent dose, solution pH, and coagulant concentration. Each variable was examined at three levels (-1, 0, +1) (Table 2). The range of the variables was determined according to some preliminary tests as well as relevant existing reports [43]. The following quadratic equation describes the best mathematical relationship between the variable parameters and the adsorption efficiency of the process:

$$y_{\text{Pred}} = \beta_0 + \sum_i^k \beta_i x_i + \sum_i^k \beta_{ii} x_i^2 + \sum_i^{k-1} \sum_{j=i+1}^k \beta_{ij} x_i x_j + \varepsilon \quad (1)$$

where y , β_0 , β_i , β_{ii} , and β_{ij} are the predicted response, the constant coefficient, the linear coefficients, the quadratic coefficients, and the interaction coefficients, respectively; x_i and x_j are the influencing process variables; k is the number of variables, and ε is the residual error. The experiment design and the graphical analyses were carried out by a Design Expert software (version 10). The coefficient of R^2 and data of analysis of variance (ANOVA) were applied to evaluate the obtained model. Table 3 presents the corresponding designed matrix and predicted results.

2.7. Error analysis

Average absolute relative error (AARE), chi-square test (χ^2), and residual root mean square error (RMSE) were applied to measure the agreement of the empirical results with the predictions for adsorption isotherm and kinetic models. The relevant equations are presented below:

$$\text{RMSE} = \sqrt{\frac{1}{n-p} \sum_{i=1}^n (q_{e,\text{exp}} - q_{e,\text{cal}})_i^2} \quad (2)$$

$$\text{AARE} = \frac{1}{N} \sum_{i=1}^N \left[\left| \frac{(q_{e,\text{cal}} - q_{e,\text{exp}})}{q_{e,\text{exp}}} \right| \right]_i \quad (3)$$

$$\chi^2 = \sum_{i=1}^n \left[\frac{(q_{e,\text{exp}} - q_{e,\text{cal}})^2}{q_{e,\text{cal}}} \right]_i \quad (4)$$

where $q_{e,\text{cal}}$ and $q_{e,\text{exp}}$ are the calculated and experimental values obtained by the model, respectively. n and p ;

Table 3
Three-factor Box–Behnken matrix and the values of the determined responses

Runs	Design factor			Response		
	pH	[GO] (mg L ⁻¹)	[FeCl ₃ ·6H ₂ O] (mg L ⁻¹)	CIP removal (%)	q_e (mg g ⁻¹)	Turbidity (NTU)
1	10	80	5.5	41.0	51.0	13
2	3	4	5.5	5.5	137.1	18
3	3	42	1	60.5	144	12
4	6.5	4	10	9.2	229.2	19
5	6.5	80	10	83.9	105	9
6	6.5	80	1	81.7	102.1	9
7	6.5	42	5.5	54.5	129.7	7
8	6.5	4	1	13.6	339.3	16
9	3	42	10	57.8	137.7	17
10	6.5	42	5.5	67.3	160.2	14
11	10	4	5.5	8.0	199.7	17
12	6.5	42	5.5	70.6	168.0	6
13	10	42	10	38.4	91.4	7
14	3	80	5.5	82.5	103.1	6
15	6.5	42	5.5	56.5	134.6	13
16	10	42	1	21.7	51.7	10
17	6.5	42	5.5	61.7	147.0	12

respectively, represent the numbers of empirical data and model variables. RMSE and AARE should have the smallest possible values. Chi-square (χ^2) is employed to detect the best model. The best model is the one that yields the lowest error function value [44].

2.8. General procedure

The CIP adsorption by adsorbents (GO and rGO) in the presence or absence of Fe₃O₄ nanoparticles was applied using a batch procedure. All of the experiments were performed using a 1,000 mL glass flask stirred using a magnetic stirrer with a stirring rate of 200 rpm. For each run, a calculated amount of the coagulant agent and adsorbent powder was mixed with 0.5 mL of 10,000 mg L⁻¹ CIP aqueous stock solution. Afterward, the appropriate amount of NaOH or HCl solution (of 0.1 mol L⁻¹) was applied to adjust the pH. The final volume of the samples was 500 mL. The jar-test experiments were performed on samples. After 1 h, the adsorption of CIP and turbidity were investigated. The concentration of CIP solution was 10 mg L⁻¹. The samples (10 mL) were withdrawn from the reaction vessel at predetermined times. The CIP concentration was determined with HPLC (Agilent, 1100). The amount of adsorbed CIP was calculated by determining the difference between the initial and equilibrium concentration in the aqueous solution. Eqs. (5) and (6) were used to obtain the removal efficiency and the sorption capacity of the adsorbent, respectively:

$$\text{Removal efficiency} = \frac{C_0 - C_e}{C_0} \times 100 \quad (5)$$

$$q_e = \frac{(C_0 - C_e)V}{m} \quad (6)$$

where C_0 and C_e are the initial and equilibrium concentrations of CIP in mg L⁻¹, respectively, V is the volume of the CIP solution in L, and m is the dry mass of the sorbent in g.

In this work, the efficacy of rGO on CIP adsorption was also investigated, and finally, the best adsorbent was selected. In addition to the parameters included in the RSM, the effects of the other variables, including TDS and contact time, on the adsorption of CIP were evaluated. The sample solutions containing different amounts of dissolved solids such as NaHCO₃, KCl, Ca(NO₃)₂, and MgSO₄ were used to investigate the effects of TDS. Also, the effect of the Fe₃O₄ nanoparticle dosage on the sedimentation rate and sludge volume was studied. In addition, various isotherm equations were used for explaining the equilibrium of the CIP adsorption. These equations show the relationship between the equilibrium concentration of CIP in the adsorbent and the solution. Also, several models, including pseudo-zero-order, pseudo-first-order, and pseudo-second-order were investigated at 298 K to determine the sedimentation kinetics of sludge. It should be noted that all the studies in this section were conducted under optimum conditions.

3. Results and discussion

3.1. Characterization of GO and Fe₃O₄ nanoparticles

The SEM image, XRD pattern, and FTIR spectrum of as-synthesized GO are shown in Fig. 1b, d, and f, respectively. The nanosheets of the synthesized GO can be seen in Fig. 1b. The XRD pattern for GO in Fig. 1d indicated a

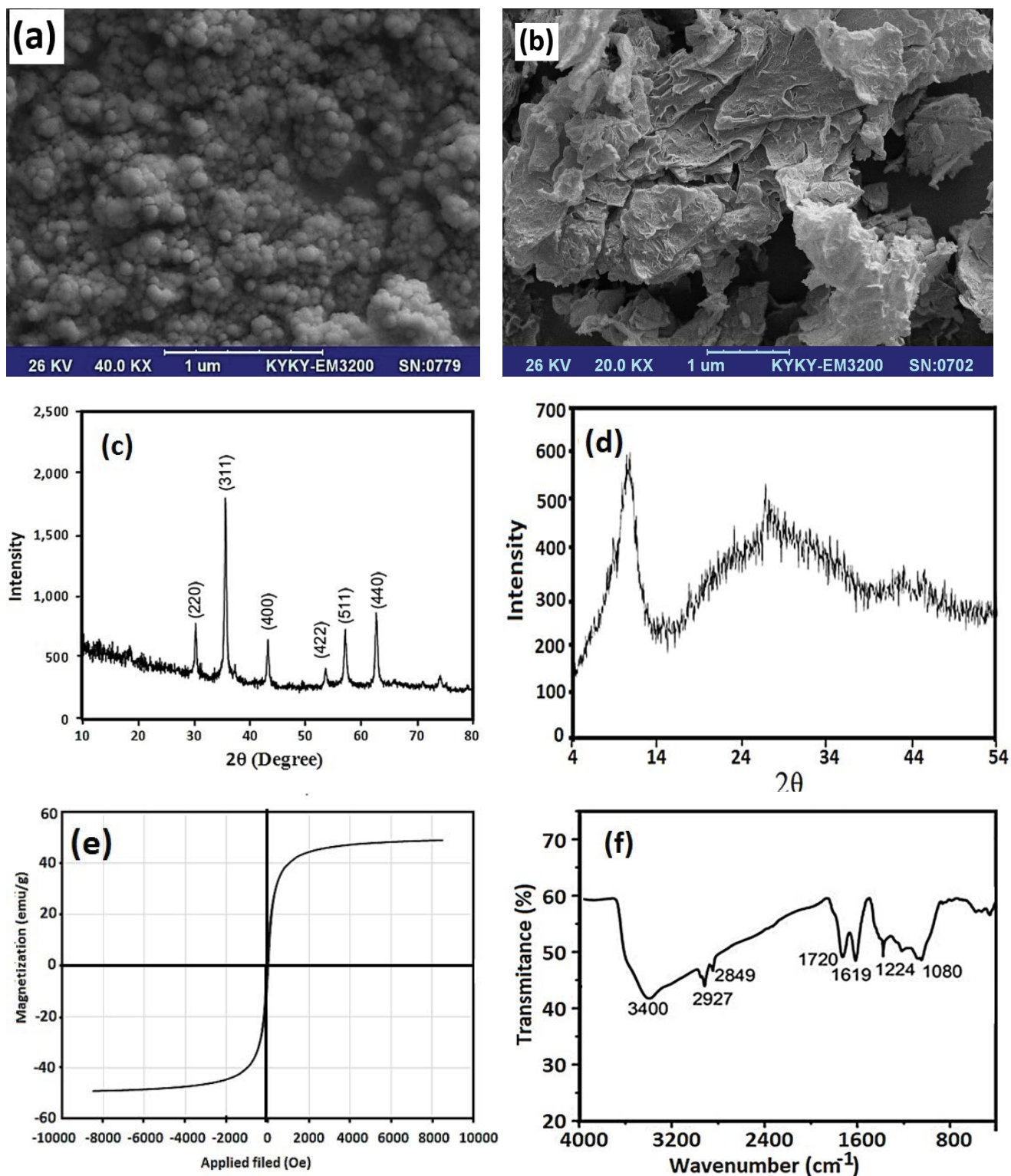


Fig. 1. SEM image (a), XRD pattern (c), and magnetization curve of the magnetite nanoparticle (e); SEM images (b), XRD pattern (d), and FTIR spectrum of the synthesis GO (f).

wide peak at 10.92° , which could be attributed to the standard XRD pattern [45]. Furthermore, an FTIR analysis was employed to specify the surface functional groups of GO. Fig. 1f shows the FTIR spectrum of GO. The wide peak at $3,400\text{ cm}^{-1}$ is related to the O–H group. The absorption peaks at $1,619$; $1,224$ and $1,080\text{ cm}^{-1}$ are ascribed to C=O, C–C, and C–O vibrations, respectively [46].

The as-synthesized Fe_3O_4 nanoparticles were investigated using SEM, XRD, and VSM analyses, and the results are presented in Fig. 1a, c, and e. The results of the SEM analysis (Fig. 1a) showed that the average diameter of the synthesized Fe_3O_4 was smaller than 50 nm . The XRD pattern of the Fe_3O_4 nanoparticles, presented in Fig. 1c, shows that the diffraction peaks at 30.2° (220), 35.5° (311), 43.2° (400), 53.5° (422), 57.2° (511), and 62.7° (440) were consistent with the standard XRD pattern of Fe_3O_4 (JCPDS, no. 65-3107) [47]. The magnetization curves in Fig. 1e give a saturation magnetization value of 40 emu g^{-1} for the Fe_3O_4 nanoparticles at room temperature. This value indicates that Fe_3O_4 nanoparticles can be easily separated by a magnet. In addition, zeta potential analysis was used for the adsorbent. Zeta potential, which is effective on the stability of nanoparticles, depends on the surface charge. For GO, the zeta potential value varied from -26.7 to -9.3 mV after the jar test. Apparently, the coagulation and the flocculation process greatly affect the neutralization of the surface charge of particles.

3.2. Effect of hydrazine content on the adsorption capacity of GO

To examine the effect of hydrazine on the adsorption capacity of CIP, a series of experiments were conducted using different concentrations of hydrazine as the reducing agent (0.04 , 0.08 , and 0.16 mg L^{-1}) for reduction of GO.

The adsorption capacities of GO and rGO are compared in Fig. 2. The results indicate that the highest adsorption capacity is related to GO (226 mg L^{-1}), and the rGOs adsorption capacity was reduced by raising the hydrazine content. The reduction of GO can lead to a change in the surface structure of GO. The removal of oxygen functional groups as the result of the chemical reduction can lead to the elimination of the GO electrostatic interactions, which is important for CIP adsorption. On the other hand, aggregation of

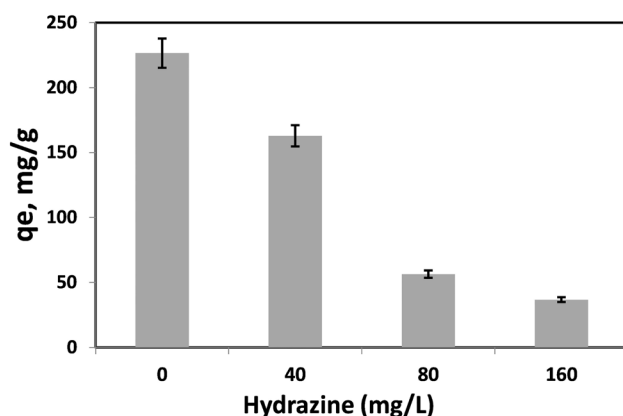


Fig. 2. Effect of hydrazine on the adsorption capacity of GO.

the adsorbent particles after the reduction process may be a reason for the decrease in CIP adsorption capacity.

3.3. Effect of contact time

Contact time is an essential parameter in the removal process. In order to understand the effect of time, the adsorption amount and removal efficiency were investigated within 1–30 min, the results are presented in Fig. 1S. The experiments were done at a CIP concentration of 10 mg L^{-1} , pH 6.0, GO dose of 0.08 mg L^{-1} , and $\text{FeCl}_3 \cdot 6\text{H}_2\text{O}$ value of 10 mg L^{-1} . The adsorption amount and the removal efficiency increased with increasing contact time to 2 min, and then remained almost constant, showing a rapid adsorption rate, which could have arisen from the high electrostatic interaction between the charged surface of the adsorbent and CIP ionic species. Although the highest adsorption rate and removal efficiency was obtained at a contact time of 2 min, the turbidity removal was low. Therefore, the optimum contact time of 15 min was selected to achieve the maximum reduction in CIP and turbidity.

3.4. Central composite design (CCD) model results for CIP adsorption

The results in Table 4 show that the removal efficiency varied from 5.5% to 84.0% under different conditions. Model fitting was used to obtain the best mathematical expression that can describe the obtained removal efficiencies. A quadratic mathematical expression showing the removal efficiency as a function of the adsorbent dosage, initial pH, and coagulant agent concentration was developed (Eq. 7)

$$\begin{aligned} \text{CIP Removal \%} = & -34.43702 + 14.98 \times A + 2.07 \times B - 1.58 \\ & \times C - 0.083 \times AB + 0.428 \times AC - 0.012 \times BC - 1.31276A^2 \\ & - 8.16 \times B^2 - 0.023 \times C^2 \end{aligned} \quad (7)$$

The data of analysis of variance (ANOVA) were applied to evaluate the significance of the regression model and the effect of the factors. The parameters having a p -value smaller than 0.05 were considered statistically significant. In this study, all model parameters were significant except for the terms BC and C^2 , which were eliminated. The prob. $> F$ values smaller than 0.0001 and the F -value of 50.17 indicate that this model is significant. Also, the lack-of-fit F -value of 0.36 and the p -value of 0.85 imply the lack-of-fit is not significant compared to the pure error. Furthermore, the Adj- R^2 and Pred- R^2 values were 0.9556 and 0.9243, respectively. Both values were found to be close to the corresponding R^2 value of 0.9750, confirming that the model is accurate. Table 5 presents the empirical and predicted amounts for the CIP removal efficiency percentage, which indicated great consistency between the predicted and experimental results. The accuracy of the model was proven by several statistical items, resulting in a significant model that can be applied to predict the CIP removal efficiency using GO.

3.5. Effects of the variables on the removal efficiency

The perturbation plot can be applied to show the effect of all the factors and compare them at any point within

Table 4
The data of ANOVA for the quadratic response model*

Source	Sum of squares	Degrees of freedom	Mean square	F-value	Prob. > F	
Model	10,664.42	7	1,523.49	50.17	<0.0001	Significant
A-pH	1,001.06	1	1,001.06	32.97	0.0003	
B-GO	7,085.86	1	7,085.86	233.37	<0.0001	
C-FeCl ₃ ·6H ₂ O	147.06	1	147.06	4.84	0.0553	
AB	482.90	1	482.90	15.90	0.0032	
AC	181.44	1	181.44	5.98	0.0371	
A ²	1,088.53	1	1,088.53	35.85	0.0002	
B ²	583.57	1	583.57	19.22	0.0018	
Residual	273.27	9	30.36			
Lack of fit	85.48	5	17.10	0.36	0.8512	Not significant
Pure error	187.79	4	46.95			
Cor. total	10,937.70	16				

R² = 0.9750, Adj-R² = 0.9556, Pred-R² = 0.9243

Table 5
Isotherm variables found with linear regression and error values for CIP adsorption on to GO at 298 K

Isotherm	Equation	Parameters	Errors
Langmuir	$\frac{q_e}{C_e} = \frac{1}{k_L q_m} + \frac{C_e}{q_m}$ (8)	q_m : 185 mg L ⁻¹ ; k_L : 0.46 L mg ⁻¹	R ² = 0.99; RMSE = 4.44; AARE = 0.03; χ^2 = 0.62
Freundlich	$\ln q_e = \ln k_F + \frac{1}{n} k_F$ (9)	n_F : 2.2; k_F : 59.92 (mg g ⁻¹) (L mg ⁻¹) ^{1/n}	R ² = 0.98; RMSE = 8.39; AARE = 0.05; χ^2 = 1.58
Temkin	$q_e = B_1 \ln A + B_1 \ln C_e$ (10)	B_1 : mg g ⁻¹ ; A : L mg ⁻¹	R ² = 0.99; RMSE = 5.48; AARE = 0.05; χ^2 = 0.85
	$\ln q_e = \ln q_s - \beta \epsilon^2$ (11)	q_s : 136.49 mg g ⁻¹	R ² = 0.98
Dubinin–Radushkevich	$\epsilon = RT \ln \left(1 + \frac{1}{C_e} \right)$ (12)	β : 3.45 × 10 ⁻⁷ mol ² J ⁻¹	RMSE = 11.59; AARE = 0.07; χ^2 = 3.41

q_m : maximum adsorption capacity reflecting a complete monolayer (mg g⁻¹), k_L : Langmuir constant or adsorption equilibrium constant (L mg⁻¹), n : isotherm constant showing the empirical parameter, k_F : {(mg g⁻¹) (L mg⁻¹)^{1/n}} Freundlich isotherm constant showing the capacity parameter, A_1 : (L mg⁻¹) and B_1 (L mg⁻¹) Temkin constants, q_s : adsorption capacity (mg g⁻¹), β : constant of Dubinin–Radushkevich (mol² J⁻²), R : 8.314 gas constant (J mol⁻¹ K⁻¹), T : absolute temperature (K).

the designed space. Fig. 3 presents the perturbation plot, which indicates all the factors have a considerable influence on the CIP removal efficiency. The removal efficiency was improved by an increase in the adsorbent dose because of an increase in active sites and available surface area for adsorbing CIP, while at a lower amount of the adsorbent, adsorption efficiency decreases because of the high ratio of CIP molecule to the vacant site [48,49]. However, a reduction in the removal efficiency was observed as the pH increased because of the repulsion force between the anionic form of CIP and GO with anionic active sites at alkaline pHs [20]. As can be seen in the perturbation plot, the efficacy of coagulant agent concentration on the CIP removal efficiency is not very significant. However, a slight increase can be due to charge neutralization of GO surface using Fe³⁺ ions,

thereby reducing the repulsive force between GO and CIP. On the other hand, the results showed that pH and the GO amount were rather more influential parameters than the coagulant agent factor on the removal efficiency.

3.6. Effect of independent parameters and their interactions

The 3D plots (Fig. 4a and c) and related contours (Fig. 4b and d) were used to show the influence of the operating parameters and their interactions on the response. In each plot, two operating parameters were changed within the experimental ranges (-1, 0, and +1), whereas the other was kept constant at a specific level (zero). Fig. 4a and c indicate the interactive effect of the dosages of GO and pH. When the GO dosage was high, the removal efficiency decreased by

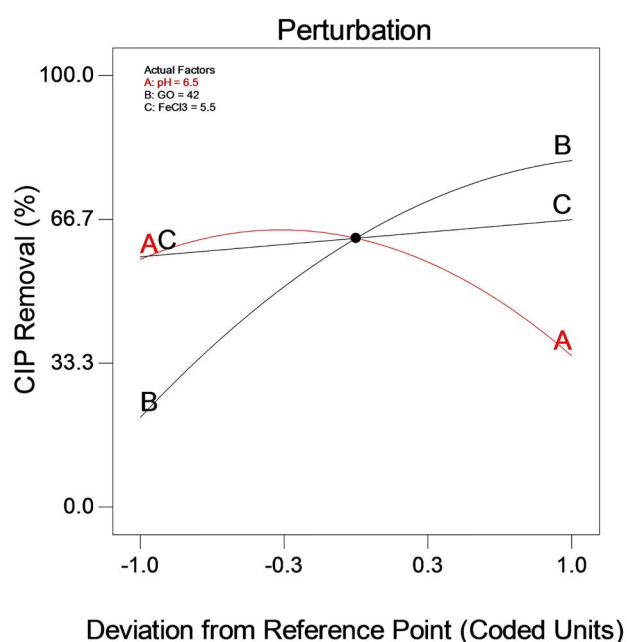


Fig. 3. Perturbation plots for removal of CIP by GO.

raising the pH, which may have arisen from an increase in the electrostatic repulsions between GO surface and anionic form of CIP [20]. However, when the GO dosage was low, increasing the initial pH to about 6.5 increased the removal efficiency until the maximal point and then a mild reduction was achieved. In addition, Fig. 4a shows that by increasing the GO dosage at low pH, the removal efficiency increased significantly, which can be attributed to a rise in the active site amount of GO [48,49].

Fig. 4b and d show the removal efficiency variations as a function of the coagulant agent ($\text{FeCl}_3 \cdot 6\text{H}_2\text{O}$) dosage and pH at the GO levels of -1, 0, and +1. As can be seen, the removal efficiency increased by increasing the pH up to about 5; however, an adverse effect was observed when the pH was further increased. The pH effect can be explained by the charge variation on the GO surface. It is known that at the pH of 3, the main carboxylic groups are neutral. At acidic pHs, the electrostatic attraction between CIP and GO is weak due to the nature of the surface charge of both species [20]. Furthermore, an increase in the solubility of CIP at acidic pHs may be another reason for a decrease in the CIP removal efficiency. However, at pHs around 5, the carboxylic groups (about 80%) converted to $-\text{COO}^-$ with a negative charge. For confirming this mechanism, the zeta potential of GO particles was determined, and the results showed the zeta potential of -16 mv at pH 8. Therefore, there is an attraction between the GO surface and cationic CIP species. Instead, at alkaline pHs, the repulsion force between the anionic form of CIP and GO with anionic active sites is the reason for the reduction in the removal efficiency of CIP.

Under the optimum conditions (GO dosage of 0.08 mg L^{-1} , pH of 6.0, and $\text{FeCl}_3 \cdot 6\text{H}_2\text{O}$ concentration of 10 mg L^{-1}), maximum removal of 84.0% was predicted using the model. To confirm the accuracy of the model, the optimized process was conducted on the sample solution containing 10 mg L^{-1}

of CIP, and the results showed a removal efficiency of 83.1%, which confirmed the reliability of the model.

3.7. Effect of TDS

To study the effect of TDS on CIP adsorption using GO, solutions with various concentrations of dissolved solids within the $0\text{--}1,000 \text{ mg L}^{-1}$ range were prepared. The initial CIP concentration was retained at 10 mg L^{-1} . The coagulation process was conducted at pH 6.0 and $\text{FeCl}_3 \cdot 6\text{H}_2\text{O}$ concentration of 10 mg L^{-1} . A stock solution of TDS (1000 mg L^{-1}) with the composition presented in Table 1S was produced by dissolving proper amounts of related solids in deionized water. The results showed that the adsorption performance slightly increased by increasing TDS; however, at TDS levels higher than 800 mg L^{-1} , removal efficiency decreased. GO can adsorb CIP through electrostatic interaction between the surface carboxylic groups and amine groups of CIP. It can be proposed that increasing the salt concentration can lead to blocking the adsorption sites, thereby decreasing the electrostatic interaction between the amine groups of CIP and surface functional groups (carboxylic) of GO. The competition for adsorption on the active sites of the adsorbent between the CIP cationic species and other inorganic cations may be another reason for the reduction in the removal efficiency.

3.8. Effect of initial CIP concentration

The initial concentration of pollutants is a crucial parameter in the removal efficiency. Several experiments were carried out at different initial CIP concentrations in the range of $5\text{--}25 \text{ mg L}^{-1}$. Fig. 5 illustrates that the removal efficiency declined as the initial CIP concentration increased since there are more CIP ions than the active sites on the adsorbent. On the other hand, when the CIP concentration increased, the CIP adsorption increased. Consequently, a high CIP concentration is more favorable for CIP adsorption.

3.9. Adsorption isotherms

The equilibrium adsorption isotherm model shows the interactive behavior between the equilibrium concentrations of the adsorbate and adsorbent. The most commonly used equilibrium isotherms were Langmuir, Freundlich, Temkin, and Dubinin–Radushkevich. The equilibrium adsorption experiments were carried out by shaking the solutions with different initial CIP concentrations ($5\text{--}25 \text{ mg L}^{-1}$) at the optimum conditions (GO: 0.08 mg L^{-1} , $\text{FeCl}_3 \cdot 6\text{H}_2\text{O}$: 10 mg L^{-1} , pH: 6.0, and T : 25°C). The CIP concentration was determined after the jar test and adsorbent separation. The mentioned models were employed for the analyses of the equilibrium data. Table 5 represents the linear forms of the applied models and the achieved results. According to R^2 values, Temkin and Langmuir models fitted the data well. With respect to AARE, RMSE, and χ^2 values, the Langmuir model exhibited smaller error values than the other models; thus, the Langmuir isotherm was considered to be the best fitting model, suggesting that the adsorbent surface is homogeneous and the adsorption film has a monolayer coverage [50]. This can be explained

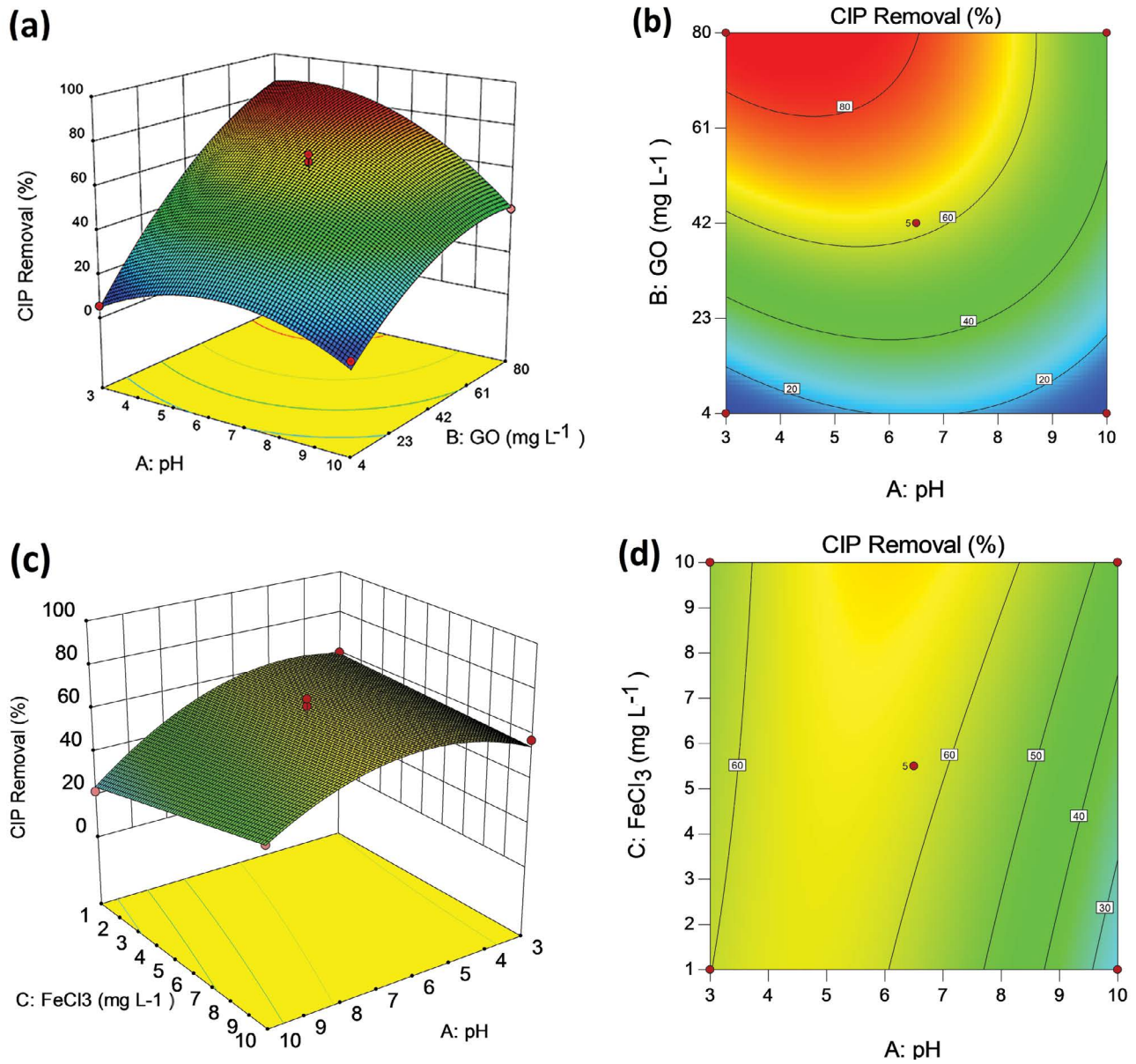


Fig. 4. The 3D plots for interaction effect of (a) pH and GO amount; FeCl₃·6H₂O concentration at the level of +1 (b) FeCl₃·6H₂O concentration and pH; GO at the level of +1.

Table 6

Comparison of adsorption capacity of the prepared adsorbent with those of other reported adsorbents

Adsorbent	q_{\max} (mg g ⁻¹)	References
Porous Zn/Fe based layered double hydroxides	344.8	[51]
Amine-functionalized MCM-41 mesoporous silica	164.3	[52]
Ga ₂ S ₃ /S-modified biochar	330.2	[53]
Materials prepared from Moroccan oil shales	81.1	[54]
Thermally modified bentonite clay	114.4	[55]
Activated carbons based folium cycas	204.0	[56]
Nanocellulose extracted from grass	227.2	[57]
GO	185	This research

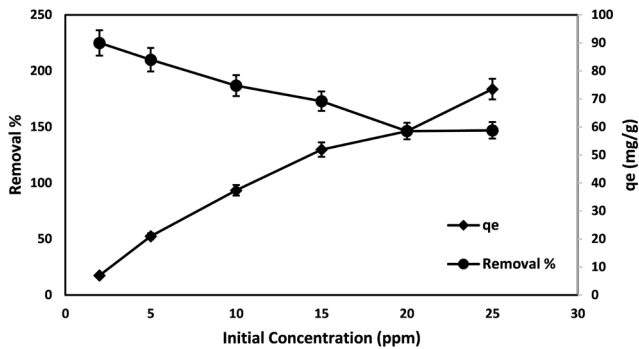


Fig. 5. Effect of initial concentration of CIP on adsorption capacity and removal efficiency: pH = 5.5, [GO] = 0.04 mg L⁻¹, [FeCl₃·6H₂O] = 10 mg L⁻¹, contact time = 15 min and stirring rate = 150 rpm.

by the homogeneous adsorption of monolayer CIP onto the active sites of the GO adsorbent. The maximum adsorption capacity obtained using the Langmuir model was 185 mg g⁻¹.

The adsorption capacity of the adsorbent in this research was compared with those reported for other adsorbents (Table 6). As can be seen, the maximum adsorption capacity of the prepared adsorbent is nearly close to those of the most reported adsorbents.

3.10. Effect of Fe₃O₄ concentration on sedimentation and kinetic study

To evaluate the influence of the concentration of the Fe₃O₄ nanoparticles on the sludge sedimentation, the ISSMI process was investigated by adding the different volumes of Fe₃O₄ solution (6,000 mg L⁻¹) in the range of 0 to 3 to 500 mL of the solution containing 10 mg L⁻¹ of CIP. After the jar test experiments, the solution samples were placed on the neodymium magnet (5 cm × 5 cm × 4cm) and the turbidity was measured at various time intervals. Fig. 6a shows a decrease in the sludge sedimentation time from 10 to 6 min when the amount of Fe₃O₄ nanoparticles increased

Table 7

Effect of magnetic nanoparticles and anionic polyacrylamide on the sludge sedimentation rate constants (Fe₃O₄ 6,000 mg L⁻¹, FeCl₃·6H₂O: 1,000 mg L⁻¹)

Model	Fe ₃ O ₄ volume		
	0 mL	1 mL	3 mL
Pseudo-zero-order (NTU min ⁻¹)	10.15	42.42	135.4
Pseudo-first-order (min ⁻¹)	0.22	0.61	1.16
Pseudo-second-order (NTU ⁻¹ min ⁻¹)	0.004	0.0156	0.0296

from 1 to 3 mL. However, the turbidity reached zero in a shorter time. In other words, the Fe₃O₄ nanoparticles have a considerable effect on the sludge sedimentation rate. It is noteworthy that in the absence of Fe₃O₄ nanoparticles, the turbidity value did not reach zero even after 60 min.

Three kinetic models including pseudo-zero-order, pseudo-first-order, and pseudo-second-order were used to investigate the sedimentation rate. Table 7 presents the linear forms of the models and the results of the calculated kinetic parameters. The results show that the rate constant increased by increasing the amount of Fe₃O₄ as a magnetic impregnation agent. The correlation coefficient for the sedimentation process by adding 3 mL of 6,000 mg L⁻¹ Fe₃O₄ was greater for the pseudo-first-order model than the other kinetic models employed. Table 2S contains the corresponding values for χ², AARE, and RMSE, which confirmed that the sedimentation process with Fe₃O₄ follows the pseudo-first-order kinetic model.

As can be seen in Table 2S, the sedimentation process without Fe₃O₄ in the presence of FeCl₃·6H₂O does not comply with any of the models investigated. Subsequently, the sludge volume index (SVI) was measured after the sedimentation process. A significant reduction in SVI occurred by adding the magnetic impregnation agent (Fe₃O₄) as a result of the magnetic force. Therefore, the magnetic Fe₃O₄ nanoparticle is capable of decreasing the sedimentation time and sludge volume index (Fig. 6b).

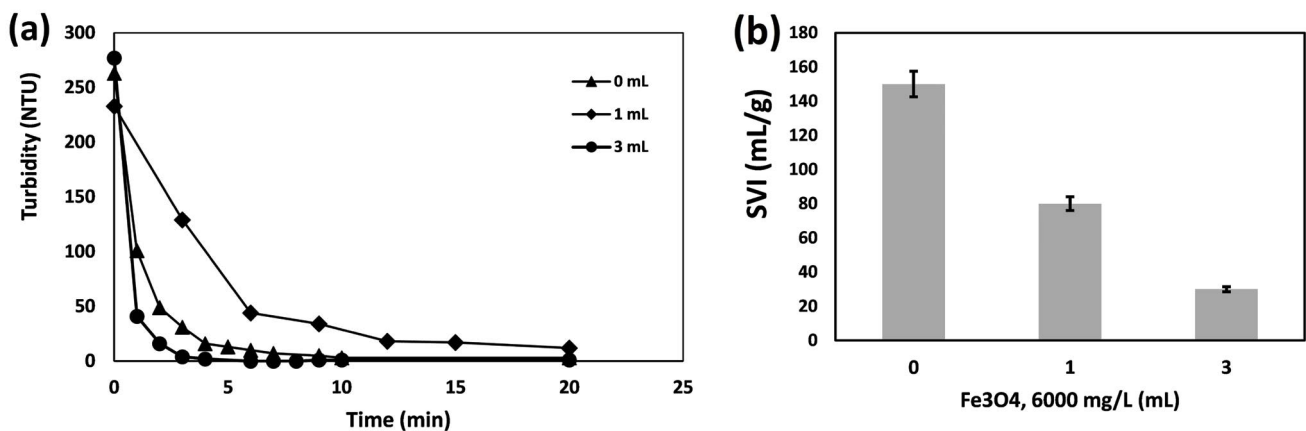


Fig. 6. Effect of the Fe₃O₄ nanoparticle on the sludge sedimentation rate and SVI: volume of sample = 1 L, [CIP] = 10 mg L⁻¹, [GO] = 0.08 mg L⁻¹, pH: 6.0, [Fe₃O₄] = 6,000 mg L⁻¹, [FeCl₃·6H₂O] = 1,000 mg L⁻¹, contact time = 15 min and stirring rate = 150 rpm.

3.11. Reusability study

To investigate the reusability potential of the GO desorption, the exhausted sludge was regenerated using an HCl solution (5% w/w). The suspension was sonicated and then the GO adsorbent was separated using centrifuging for 5 min. The removal of CIP decreased from 93.45% in the first run to 75.98% in the second run and 64.86% in the third run that indicated that GO can be reused several times without impressive loss of activity, thereby reducing the cost of the process. The adsorption capacity reduced from 116.8 to 81.0 mg g⁻¹ after the third reuse cycle.

4. Conclusions

This study evaluated the efficiency of GO and rGO adsorbents applied in the coagulation–flocculation process for ciprofloxacin (CIP) removal from surface water. Furthermore, the application of Fe₃O₄ for enhancing sedimentation rate was investigated. The results showed that the functional groups of GO have a significant impact on the adsorption of CIP, and chemical reduction of GO resulted in reducing the adsorption capacity. Among the investigated parameters, pH and the GO amount were rather more influential parameters than the coagulant agent factor on the removal efficiency. A reduction in the removal efficiency was observed as the pH increased because of the repulsion force between the anionic form of CIP and GO with anionic active sites at alkaline pHs. The maximum removal of 83.1% was obtained at an initial CIP concentration of 10 mg L⁻¹ under the optimum operating conditions (GO: 0.08 mg L⁻¹, pH: 6.0, and FeCl₃·6H₂O: 10 mg L⁻¹). The experimental equilibrium data were consistent with the Langmuir adsorption isotherm. The maximum adsorption capacity of 185 mg g⁻¹ was achieved for GO. The removal efficiency decreased slightly by increasing TDS at concentrations higher than 800 mg L⁻¹. This decline may be due to the competition between the CIP species and ions for adsorption on the GO surface. The magnetite content was a significant factor in increasing the sedimentation rate and decreasing the sludge volume. The results showed that the sludge sedimentation rate can be explained with a pseudo-first-order kinetic model. The sedimentation rate constant increased from 0.004 to 0.0296 NTU⁻¹ min⁻¹ by adding 3 mL of Fe₃O₄ nanoparticles (6,000 mg L⁻¹) to 500 mL of sample. An HCl solution with a concentration of 5% w/w was a good desorption agent for regeneration. After three cycles, the removal efficiency declined to 65%. In conclusion, GO can be applied as a potential adsorbent in a coagulation–flocculation process for enhancing the unit performance for CIP removal from surface water, and the dose of Fe₃O₄ nanoparticles is effective in sedimentation rate and sludge volume reduction. However, the development of a technology for the separation of magnetic nanoparticles in real water treatment plants is required so that their application is transferred to the related industry.

Acknowledgment

This work was supported by the grant supported by the School of Environment, College of Engineering, University of Tehran, Tehran, Iran.

References

- [1] Z. Aksu, Ö. Tunç, Application of biosorption for penicillin G removal: comparison with activated carbon, *Process Biochem.*, 40 (2005) 831–847.
- [2] D. Balarak, Y. Mahdavi, F. Mostafapour, Application of alumina-coated carbon nanotubes in removal of tetracycline from aqueous solution, *Br. J. Pharm. Res.*, 12 (2016) 1–11.
- [3] G.D. Singh, K.C. Gupta, Photo and UV degradation of ciprofloxacin antibiotic, *Int. J. Curr. Microbiol. Appl. Sci.*, 3 (2014) 641–648.
- [4] T.S. Khokhar, F.N. Memon, A.A. Memon, F. Durmaz, S. Memon, Q.K. Panhwar, S. Muneer, Removal of ciprofloxacin from aqueous solution using wheat bran as adsorbent, *Sep. Sci. Technol.*, 54 (2019) 1278–1288.
- [5] H.G. Guo, N.Y. Gao, W.H. Chu, L. Li, Y.J. Zhang, J.S. Gu, Y.L. Gu, Photochemical degradation of ciprofloxacin in UV and UV/H₂O₂ process: kinetics, parameters, and products, *Environ. Sci. Pollut. Res.*, 20 (2013) 3202–3213.
- [6] K. Kummerer, A. Al-Ahmad, V. Mersch-Sundermann, Biodegradability of some antibiotics, elimination of the genotoxicity and affection of wastewater bacteria in a simple test, *Chemosphere*, 40 (2000) 701–710.
- [7] P.-H. Chang, W.-T. Jiang, Z. Li, C.-Y. Kuo, Q. Wu, J.-S. Jean, G. Lv, Interaction of ciprofloxacin and probe compounds with palygorskite PFI-1, *J. Hazard. Mater.*, 303 (2016) 55–63.
- [8] X. Xu, J. He, Y. Li, Z. Fang, S. Xu, Adsorption and transport of ciprofloxacin in quartz sand at different pH and ionic strength, *Open J. Soil Sci.*, 4 (2014) 407–416.
- [9] K. Kummerer, Significance of antibiotics in the environment title, *J. Antimicrob. Chemother.*, 52 (2003) 5–7.
- [10] S.S. Saygi, D. Battal, The importance of drug wastes from the standpoint of environment and human health, *Marmara Pharm. J.*, 16 (2012) 82–90.
- [11] A.J. Watkinson, E.J. Murby, S.D. Costanzo, Removal of antibiotics in conventional and advanced wastewater treatment: implications for environmental discharge and wastewater recycling, *Water Res.*, 41 (2007) 4164–4176.
- [12] T. An, H. Yang, W. Song, G. Li, H. Luo, W.J. Cooper, Mechanistic considerations for the advanced oxidation treatment of fluoroquinolone pharmaceutical compounds using TiO₂ heterogeneous catalysis, *J. Phys. Chem. A*, 114 (2010) 2569–2575.
- [13] M. Malakootian, M. Ahmadian, Removal of ciprofloxacin from aqueous solution by electro-activated persulfate oxidation using aluminum electrodes, *Water Sci. Technol.*, 80 (2019) 587–596.
- [14] H. Liang, T. Li, J. Zhang, D. Zhou, C. Hu, X. An, R. Liu, H. Liu, 3-D hierarchical Ag/ZnO@CF for synergistically removing phenol and Cr(VI): heterogeneous vs. homogeneous photocatalysis, *J. Colloid Interface Sci.*, 558 (2020) 85–94.
- [15] N. Javid, Z. Honarmandrad, M. Malakootian, Ciprofloxacin removal from aqueous solutions by ozonation with calcium peroxide, *Desal. Water Treat.*, 174 (2020) 178–185.
- [16] M. Dolatabadi, S. Ahmadzadeh, A rapid and efficient removal approach for degradation of metformin in pharmaceutical wastewater using electro-Fenton process; optimization by response surface methodology, *Water Sci. Technol.*, 80 (2019) 685–694.
- [17] U. von Gunten, Ozonation of drinking water: Part I. Oxidation kinetics and product formation, *Water Res.*, 37 (2003) 1443–1467.
- [18] Y. Abdollahi, A.H. Abdullah, U.I. Gaya, S. Ahmadzadeh, A. Zakaria, K. Shamel, Z. Zainal, H. Jahangirianb, N.A. Yusof, Photocatalytic degradation of 1,4-benzoquinone in aqueous ZnO dispersions, *J. Braz. Chem. Soc.*, 23 (2012) 236–240.
- [19] S.M.A.A. Azeez, HPLC Determination of Four Textile Dyes and Studying Their Degradation using Spectrophotometric Technique, Thesis, An-Najah National University Faculty of Graduate Studies, Submitted in Partial Fulfillment of the Requirements for the Degree of Master of Science in Chemistry, Faculty of Graduate Studies, at An-Najah National University, Nablus, Palestine, 2005, pp. 1–110. Available at: <https://doi.org/10.1017/CBO9781107415324.004>.
- [20] Z. Li, H. Hong, L. Liao, C.J. Ackley, L.A. Schulz, R.A. Macdonald, A.L. Mihelich, S.M. Emard, A mechanistic study of

- ciprofloxacin removal by kaolinite, *Colloids Surf., B*, 88 (2011) 339–344.
- [21] W.-T. Jiang, P.-H. Chang, Y.-S. Wang, Y. Tsai, J.-S. Jean, Z. Li, K. Krukowski, Removal of ciprofloxacin from water by birnessite, *J. Hazard. Mater.*, 250–251 (2013) 362–369.
- [22] N. Genç, E. Can Dogan, M. Yurtsever, Bentonite for ciprofloxacin removal from aqueous solution, *Water Sci. Technol.*, 68 (2013) 848–855.
- [23] D. Balarak, F.K. Mostafapour, A. Joghataei, Kinetics and mechanism of red mud in adsorption of ciprofloxacin in aqueous solution, *Biosci. Biotechnol. Res. Commun.*, 10 (2017) 241–248.
- [24] C.Y. Teh, P.M. Budiman, K.P.Y. Shak, T.Y. Wu, Recent advancement of coagulation–flocculation and its application in wastewater treatment, *Ind. Eng. Chem. Res.*, 55 (2016) 4363–4389.
- [25] S.F. de Aquino, E.M.F. Brandt, C.A. de L. Chernicharo, Remoção de fármacos e desreguladores endócrinos em estações de tratamento de esgoto: Revisão da literatura, *Eng. Sanit. e Ambient.*, 18 (2013) 187–204.
- [26] F.B. Queiroz, E.M.F. Brandt, S.F. Aquino, C.A.L. Chernicharo, R.J.C.F. Afonso, Occurrence of pharmaceuticals and endocrine disruptors in raw sewage and their behavior in UASB reactors operated at different hydraulic retention times, *Water Sci. Technol.*, 66 (2012) 2562–2569.
- [27] C.V. Faria, G.C. Moreira, A.P.B. Araújo, L.E. Marques, L.P. Oliveira, B.C. Ricci, M.C.S. Amaral, F.V. Fonseca, Integration of ozonation and an anaerobic expanded granular sludge bed reactor for micropollutant removal from sewage, *Environ. Sci. Pollut. Res.*, 28 (2020) 23778–23790.
- [28] V. Matamoros, V. Salvador, Evaluation of a coagulation/flocculation–lamellar clarifier and filtration–UV–chlorination reactor for removing emerging contaminants at full-scale wastewater treatment plants in Spain, *J. Environ. Manage.*, 117 (2013) 96–102.
- [29] M.E.R. Jalil, M. Baschini, K. Sapag, Removal of ciprofloxacin from aqueous solutions using pillared clays, *Materials (Basel)*, 10 (2017) 17–19.
- [30] J.A. González, M.E. Villanueva, L.L. Piehl, G.J. Copello, Development of a chitin/graphene oxide hybrid composite for the removal of pollutant dyes: adsorption and desorption study, *Chem. Eng. J.*, 280 (2015) 41–48.
- [31] Y. Li, Q. Du, T. Liu, X. Peng, J. Wang, J. Sun, Y. Wang, S. Wu, Z. Wang, Y. Xia, L. Xia, Comparative study of methylene blue dye adsorption onto activated carbon, graphene oxide, and carbon nanotubes, *Chem. Eng. Res. Des.*, 91 (2013) 361–368.
- [32] B. Yu, X. Zhang, J. Xie, R. Wu, X. Liu, H. Li, F. Chen, H. Yang, Z. Ming, S.-T. Yang, Magnetic graphene sponge for the removal of methylene blue, *Appl. Surf. Sci.*, 351 (2015) 765–771.
- [33] Y. Zhuang, F. Yu, J. Chen, J. Ma, Batch and column adsorption of methylene blue by graphene/alginate nanocomposite: comparison of single-network and double-network hydrogels, *J. Environ. Chem. Eng.*, 4 (2016) 147–156.
- [34] P. Arabkhani, H. Javadian, A. Asfaram, M. Ateia, Decorating graphene oxide with zeolitic imidazolate framework (ZIF-8) and pseudo-boehmite offers ultra-high adsorption capacity of diclofenac in hospital effluents, *Chemosphere*, 271 (2021) 129610, doi: 10.1016/j.chemosphere.2021.129610.
- [35] P. Arabkhani, A. Asfaram, M. Ateia, Easy-to-prepare graphene oxide/sodium montmorillonite polymer nanocomposite with enhanced adsorption performance, *J. Water Process Eng.*, 38 (2020) 101651, doi: 10.1016/j.jwpe.2020.101651.
- [36] P.N. Diagboya, B.I. Olu-Owolabi, K.O. Adebowale, Synthesis of covalently bonded graphene oxide–iron magnetic nanoparticles and the kinetics of mercury removal, *RSC Adv.*, 5 (2015) 2536–2542.
- [37] J. Sun, Q. Liang, Q. Han, X. Zhang, M. Ding, One-step synthesis of magnetic graphene oxide nanocomposite and its application in magnetic solid-phase extraction of heavy metal ions from biological samples, *Talanta*, 132 (2015) 557–563.
- [38] P. Zong, S. Wang, Y. Zhao, H. Wang, H. Pan, C. He, Synthesis and application of magnetic graphene/iron oxides composite for the removal of U(VI) from aqueous solutions, *Chem. Eng. J.*, 220 (2013) 45–52.
- [39] S. Moharramzadeh, M. Baghdadi, In situ sludge magnetic impregnation (ISSMI) as an efficient technology for enhancement of sludge sedimentation: removal of methylene blue using nitric acid-treated graphene oxide as a test process, *J. Environ. Chem. Eng.*, 4 (2016) 2090–2102.
- [40] J. Liu, G. Liu, W. Liu, Preparation of water-soluble β -cyclodextrin/poly(acrylic acid)/graphene oxide nanocomposites as new adsorbents to remove cationic dyes from aqueous solutions, *Chem. Eng. J.*, 257 (2014) 299–308.
- [41] M. Behjati, M. Baghdadi, A. Karbassi, Removal of mercury from contaminated saline wastewaters using dithiocarbamate functionalized-magnetic nanocomposite, *J. Environ. Manage.*, 213 (2018) 66–78.
- [42] APHA/AWWA/WEF, Standard Methods for the Examination of Water and Wastewater, American Public Health Association (APHA), American Water Works Association (AWWA), Water Environment Federation (WEF), Washington DC, 2012, p. 541. Available at: [https://doi.org/ISBN 9780875532356](https://doi.org/ISBN%209780875532356).
- [43] V.A. Sakkas, M.A. Islam, C. Stalikas, T.A. Albanis, Photocatalytic degradation using design of experiments: a review and example of the Congo red degradation, *J. Hazard. Mater.*, 175 (2010) 33–44.
- [44] F. Tümeşek, Ö. Avci, Investigation of kinetics and isotherm models for the Acid orange 95 adsorption from aqueous solution onto natural minerals, *J. Chem. Eng. Data*, 58 (2013) 551–559.
- [45] G.X. Wang, J. Yang, J. Park, X.L. Gou, B. Wang, H. Liu, J. Yao, Facile synthesis and characterization of graphene nanosheets, *J. Phys. Chem. C*, 112 (2008) 8192–8195.
- [46] E.-Y. Choi, T.H. Han, J. Hong, J.E. Kim, S.H. Lee, H.W. Kim, S.O. Kim, Noncovalent functionalization of graphene with end-functional polymers, *J. Mater. Chem.*, 20 (2010) 1907–1912.
- [47] S. Mirshahghassemi, J.R. Lead, Oil recovery from water under environmentally relevant conditions using magnetic nanoparticles, *Environ. Sci. Technol.*, 49 (2015) 11729–11736.
- [48] R. Bagheri, M. Ghaedi, A. Asfaram, E. Alipanahpour Dil, H. Javadian, RSM-CCD design of malachite green adsorption onto activated carbon with multimodal pore size distribution prepared from *Amygdalus scoparia*: kinetic and isotherm studies, *Polyhedron*, 171 (2019) 464–472.
- [49] P. Arabkhani, A. Asfaram, Development of a novel three-dimensional magnetic polymer aerogel as an efficient adsorbent for malachite green removal, *J. Hazard. Mater.*, 384 (2020) 121394, doi: 10.1016/j.jhazmat.2019.121394.
- [50] E. Alipanahpour Dil, M. Ghaedi, A. Asfaram, F. Mehrabi, A.A. Bazrafshan, L. Tayebi, Synthesis and application of Ce-doped TiO₂ nanoparticles loaded on activated carbon for ultrasound-assisted adsorption of Basic red 46 dye, *Ultrason. Sonochem.*, 58 (2019) 104702, doi: 10.1016/j.ultsonch.2019.104702.
- [51] S. Sharma, G. Sharma, A. Kumar, P. Dhiman, T. Al Gami, M. Naushad, Z. AlOthman, F.J. Stadler, Controlled synthesis of porous Zn/Fe based layered double hydroxides: synthesis mechanism, and ciprofloxacin adsorption, *Sep. Purif. Technol.*, 278 (2021) 119481, doi: 10.1016/j.seppur.2021.119481.
- [52] G. Abu Rumman, T.J. Al-Musawi, M. Sillanpää, D. Balarak, Adsorption performance of an amine-functionalized MCM-41 mesoporous silica nanoparticle system for ciprofloxacin removal, *Environ. Nanotechnol. Monit. Manage.*, 16 (2021) 100536, doi: 10.1016/j.enmm.2021.100536.
- [53] X. Zheng, X. He, H. Peng, J. Wen, S. Lv, Efficient adsorption of ciprofloxacin using Ga₂S₃/S-modified biochar via the high-temperature sulfurization, *Bioresour. Technol.*, 334 (2021) 125238, doi: 10.1016/j.biortech.2021.125238.
- [54] E.H. Chafyq, K. Legrouni, M. Aghrouh, M. Oumam, S. Mansouri, E. Hassane Khouya, H. Hannache, Adsorption of ciprofloxacin antibiotic on materials prepared from Moroccan oil shales, *Chem. Phys. Lett.*, 778 (2021) 138707, doi: 10.1016/j.cplett.2021.138707.
- [55] R. Antonelli, G.R.P. Malpass, M.G.C. da Silva, M.G.A. Vieira, Adsorption of ciprofloxacin onto thermally modified bentonite

clay: experimental design, characterization, and adsorbent regeneration, *J. Environ. Chem. Eng.*, 8 (2020) 104553, doi: 10.1016/j.jece.2020.104553.

- [56] J. Kong, Y. Zheng, L. Xiao, B. Dai, Y. Meng, Z. Ma, J. Wang, X. Huang, Synthesis and comparison studies of activated carbons based folium cycas for ciprofloxacin adsorption, *Colloids Surf., A*, 606 (2020) 125519, doi: 10.1016/j.colsurfa.2020.125519.
- [57] T. Shahnaz, V. Vishnu Priyan, S. Pandian, S. Narayanasamy, Use of nanocellulose extracted from grass for adsorption abatement of Ciprofloxacin and Diclofenac removal with phyto, and fish toxicity studies, *Environ. Pollut.*, 268 (2021) 115494, doi: 10.1016/j.envpol.2020.115494.

Supplementary information

S1. Preparation of graphene oxide and reduced graphene oxide

12 g of KNO_3 was dissolved in 500 mL H_2SO_4 and the mixture was added into a triple-neck glass flask. An ice bath was used to reduce the temperature of this solution. Subsequently, 10 g of graphite was poured into the solution and mixed for 2 h. After the mixing time, 60 g of potassium permanganate were leisurely poured into the solution and then mixed for 40 min. An oil bath was used to heat this solution to 40°C for 24 h. After 24 h of mixing at 40°C , 100 mL of H_2O_2 and 400 mL of deionized water were added to the solution. The light brown precipitate was washed several times with HCl (1:1) and then several times with deionized water.

S2. Synthesis of Fe_3O_4 nanoparticles

Therefore, the following solutions were prepared: 2.92 g of $\text{FeCl}_3 \cdot 6\text{H}_2\text{O}$ and then 1.05 g of $\text{FeCl}_2 \cdot 4\text{H}_2\text{O}$ were added to 300 mL of deionized water deoxygenated by purging nitrogen for 30 min. Then 80 mL of NH_3 (25% wt) was added to the above mixture dropwise within 30 min and then mixed vigorously and under nitrogen at 80°C . The precipitate

Table 1S

Effect of TDS concentration on CIP adsorption process

TDS (mg L^{-1})	Removal (%)	q_e (mg g^{-1})
300	73.63	92.04
600	81.36	101.70
800	82.04	102.55
1,000	67.69	84.61

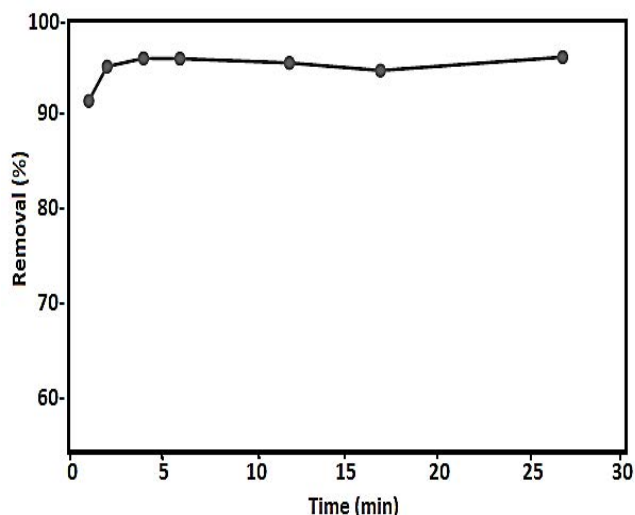


Fig. 1S. Removal efficiency of CIP dependent to contact time: $[\text{CIP}] = 10 \text{ mg L}^{-1}$, $[\text{GO}] = 0.08 \text{ mg L}^{-1}$, pH: 6.0, $[\text{FeCl}_3] = 10 \text{ mg L}^{-1}$, $T = 298 \text{ K}$, and stirring rate = 150 rpm.

magnetite nanoparticles were separated from the solution by an external magnet and washed using 100 mL of deoxygenized water.

Table 2S

Error values for sludge sedimentation of CIP on GO with and without Fe_3O_4^* and FeCl_3^{**}

Additive	Pseudo-zero-order				Pseudo-first-order				Pseudo-second-order			
	R^2	RMSE	AARE	χ^2	R^2	RMSE	AARE	χ^2	R^2	RMSE	AARE	χ^2
Without Fe_3O_4^*	0.86	423.98	4.72	-1,722.5	0.97	58.42	0.32	1852.9	0.96	181.72	0.52	1,634.6
1 mL Fe_3O_4	0.74	39.52	3.87	37.37	0.97	6.48	0.25	9.68	0.89	4.55	0.21	9.95
3 mL Fe_3O_4	0.86	65.11	8.98	5.34	0.98	9.73	0.25	34.52	0.92	12.61	0.36	47.27
5 mL FeCl_3	0.58	5.71	0.24	5.93	0.55	3.79	0.11	6.00	0.65	3.89	0.13	7.47